

# Enhancer mutations of Akv murine leukemia virus inhibit the induction of mature B-cell lymphomas and shift disease specificity towards the more differentiated plasma cell stage

Karina Dalsgaard Sørensen<sup>a,1</sup>, Sandra Kunder<sup>b</sup>, Leticia Quintanilla-Martinez<sup>b</sup>, Jonna Sørensen<sup>c</sup>, Jörg Schmidt<sup>c</sup>, Finn Skou Pedersen<sup>a,\*</sup>

<sup>a</sup> Department of Molecular Biology, University of Aarhus, C.F. Møllers Allé, Bldg. 130, DK-8000 Aarhus C, Denmark

<sup>b</sup> Institute of Pathology, GSF-National Research Center for Environment and Health, Neuherberg, Germany

<sup>c</sup> Department of Comparative Medicine, GSF-National Research Center for Environment and Health, Neuherberg, Germany

Received 6 October 2006; returned to author for revision 22 November 2006; accepted 8 December 2006

Available online 29 January 2007

## Abstract

This study investigates the role of the proviral transcriptional enhancer for B-lymphoma induction by exogenous Akv murine leukemia virus. Infection of newborn inbred NMRI mice with Akv induced 35% plasma cell proliferations (PCPs) (consistent with plasmacytoma), 33% diffuse large B-cell lymphomas, 25% follicular B-cell lymphomas and few splenic marginal zone and small B-cell lymphomas. Deleting one copy of the 99-bp proviral enhancer sequence still allowed induction of multiple B-cell tumor types, although PCPs dominated (77%). Additional mutation of binding sites for the glucocorticoid receptor, Ets, Runx, or basic helix–loop–helix transcription factors in the proviral U3 region, however, shifted disease induction to almost exclusively PCPs, but had no major influence on tumor latency periods. Southern analysis of immunoglobulin rearrangements and ecotropic provirus integration patterns showed that many of the tumors/cell proliferations induced by each virus were polyclonal. Our results indicate that enhancer mutations weaken the ability of Akv to induce mature B-cell lymphomas prior to the plasma cell stage, whereas development of plasma cell proliferations is less dependent of viral enhancer strength.

© 2006 Elsevier Inc. All rights reserved.

**Keywords:** Akv; Murine leukemia virus; B-cell lymphoma; Plasmacytoma; Retrovirus; Lymphomagenesis; Mouse tumor model; Transcriptional enhancer

## Introduction

While several studies report on B-lymphoma induction in mice linked to the replication of murine leukemia viruses (MLVs) and proviral insertional mutagenesis, these models are mostly based upon the spontaneous activation of Akv-like endogenous ecotropic retroviruses (Gilbert et al., 1993; Hartley

et al., 2000; Mucenski et al., 1986). We have previously reported that both Akv MLV and a derivative (Akv1–99) with just one copy of the 99-bp proviral enhancer induce various forms of mature B-cell lymphomas with high incidence and mean latencies of 1 year after injection of newborn random-bred NMRI mice, which are free of endogenous ecotropic MLVs (Lovmand et al., 1998). In a further development, we found that neonatal inoculation of an inbred NMRI strain with wildtype or nuclear factor 1 (NF1) site enhancer mutants of Akv1–99 resulted in an expansion of cells with characteristics of plasma cells (classified as plasmacytomas and plasma cell proliferations), through a disease process that we proposed may involve an antigen-stimulatory component (Sørensen et al., 2005). With a mean latency of only 6 months (Sørensen et al., 2005), this is the most rapid murine B-lymphoma model using non-acutely transforming retroviruses.

*Abbreviations:* PCP, plasma cell proliferation; LCC, large cell components; DLBCL, diffuse large B-cell lymphoma; FBL, follicular B-cell lymphoma; SMZL, splenic marginal zone lymphoma; SBL, small B-cell lymphoma; ML, myeloid leukemia with maturation; preT-LBL, pre-T-cell lymphoblastic lymphoma.

\* Corresponding author. Fax: +45 8619 6500.

E-mail address: [fsp@mb.au.dk](mailto:fsp@mb.au.dk) (F.S. Pedersen).

<sup>1</sup> Present address: Molecular Diagnostics Laboratory, Department of Clinical Biochemistry, Aarhus University Hospital, Skejby, DK-8200 Aarhus N, Denmark.

Major genetic determinants of disease specificity and potency of many MLVs have been mapped to the proviral U3 enhancer and, in some instances, to specific transcription factor binding sites in this region (Hallberg et al., 1991; Lenz et al., 1984; Nieves et al., 1997; Speck et al., 1990). In contrast, the viral genetic determinants of B-cell tumor induction by Akv/Akv1–99 are not well-characterized, although we have reported that two NF1 binding sites in the proviral enhancer are dispensable for tumor induction by Akv1–99 in inbred NMRI mice (Sørensen et al., 2005). This study is based on the hypothesis that other binding sites in the U3 promoter/enhancer region may play a significant role in Akv/Akv1–99-induced oncogenesis *in vivo*.

The 99-bp Akv enhancer contains binding motifs for Ets (LVb), Runx (AML/CBF) and basic helix–loop–helix (bHLH) transcription factors. The enhancer bHLH site ( $E_{gre}$ ) overlaps with a glucocorticoid response element (GRE), which mediates dexamethasone-induced activation of viral gene expression in cell culture (Celander et al., 1988). A second bHLH site (named  $E_{a/s}$ , also present in SL3-3) is located approximately 60 bp downstream of the enhancer. Mutating the  $E_{gre}$  and/or  $E_{a/s}$  site(s) reduces Akv and Akv1–99 enhancer activity significantly in lymphoid cell lines (Nielsen et al., 1994; Nielsen et al., 1996). The Ets,  $E_{gre}$  and GRE sites in the Akv/Akv1–99 enhancer are identical to the equivalent motifs in the closely related, and more extensively studied T-cell lymphomagenic viruses SL3-3 and MoMLV, whereas the Runx (core) site sequences of these viruses have a single nucleotide difference (Golemis et al., 1990). Mutation of any of these sites impedes tumor induction by MoMLV considerably, and for the Runx and Ets (LVb) sites also causes a partial shift in disease specificity (Speck et al., 1990). Likewise, efficient T-lymphoma induction by SL3-3 requires intact enhancer Runx sites (Ethelberg et al., 1997b; Hallberg et al., 1991; Morrison et al., 1995; Sørensen et al., 2004), whereas the Ets site is of minor importance (Nieves et al., 1997).

These findings together with the scarcity of reports of B-cell tumor induction by exogenous non-oncogene-bearing ecotropic MLVs (Lovmand et al., 1998; Sørensen et al., 2005) prompted us to investigate the oncogenic properties of several Akv-derived viruses in continuation of our earlier analysis of Akv1–99 NF1 site mutants (Sørensen et al., 2005). We here included the wildtype Akv virus with both copies of the 99-bp repeat as well as nine new Akv1–99 transcription control mutants in inbred NMRI mice. Five different binding sites (Runx, Ets,  $E_{gre}$ , GRE and  $E_{a/s}$ ) in the enhancer–promoter region of Akv1–99 were mutated individually or in different pairs. The current work is the first to address the possible role(s) in Akv1–99 pathogenicity of these five transcription factor binding sites, which except for  $E_{a/s}$  are highly conserved elements of the prototypic MLV enhancer framework (Golemis et al., 1990).

## Results

### Generation of mutant viruses

Point mutations were introduced into each of five different transcription factor binding sites (Ets, Runx, GRE,  $E_{gre}$  and  $E_{a/s}$ )

in the U3 region of Akv1–99 MLV (Fig. 1A) to investigate the possible role of these sites in viral pathogenesis. In some cases, two sites were mutated simultaneously (Runx+GRE, Runx+ $E_{gre}$ , GRE+ $E_{a/s}$ ,  $E_{gre}$ + $E_{a/s}$ ). This study used Akv1–99 rather than Akv because viral enhancer activity at least in some cases is more severely affected by single site mutations when one 99-bp repeat is deleted (Nielsen et al., 1996). Also, structural LTR changes by copy number fluctuation are less likely to arise *in vivo* during the replication of a single-copy enhancer containing virus (Lovmand et al., 1998; Sørensen et al., 2005). To examine the effect of the mutations on Akv1–99 enhancer activity, transient expression levels of a chloramphenicol acetyltransferase (CAT) reporter gene driven by wildtype or mutated U3 regions of Akv1–99 were measured in MPC11 murine plasmacytoma B cells, NALM6 human pre-B cells, L691 murine T cells and NIH 3T3 murine fibroblasts (Fig. 1B, Table 1). Each single site mutation (mEts, mRunx, mGR,  $mE_{gre}$  or  $mE_{a/s}$ ) reduced transient expression significantly (1.5- to 5-fold) in all four cell lines, clearly demonstrating that viral enhancer activity is compromised by the specific mutation used. The relative contribution of each site to Akv1–99 enhancer strength varied slightly between the cell lines. In some cases, mutation of two sites decreased expression even further (mRunx+m $E_{gre}$  and  $mE_{gre}$ + $mE_{a/s}$  in MPC11, NALM6 and NIH 3T3 cells), but such an effect was not always detected. Reduced enhancer strengths for Akv1–99 E-box mutants have been reported in an earlier study using a single nucleotide substitution in the  $E_{gre}$  and  $E_{a/s}$  site and a slightly different panel of hematopoietic cell lines (Nielsen et al., 1996). We have previously reported that the deletion of one 99-bp enhancer copy reduces transient enhancer activity ~2-fold in NIH 3T3 and NALM6 cells, causes a 2-fold increase in L691 cells, but has no effect in MPC11 cells (Lovmand et al., 1998; Sørensen et al., 2005).

### Tumor induction in inbred NMRI mice

To investigate the lymphomagenic properties of Akv, Akv1–99 and the nine Akv1–99 binding site mutants, newborn inbred NMRI mice were injected with equal amounts of infectious virus particles. Control mice were mock-injected with complete medium. All viruses induced tumors with similar incidence and mean latency periods of 5 to 7 months (Table 2 and Fig. 2). Gross pathology revealed no major differences between the viruses; the infected mice presented with enlarged spleen and enlarged lymph node(s). The thymus was generally not enlarged. In control mice, spontaneous tumor development was rare (Table 2).

Akv and Akv1–99 showed strikingly similar mean tumor latencies in the inbred NMRI strain (Table 2 and Fig. 2), similar to our previous results in random-bred NMRI mice (Lovmand et al., 1998). Mutation of the Ets motif had no effect on viral tumor latency, whereas five of the mutants (1–99mRunx, 1–99mGR, 1–99m $E_{gre}$ , 1–99m $E_{a/s}$  and 1–99mRunx+mGR) induced tumors with moderately, yet significantly shorter mean latency than Akv1–99 (Table 2 and Fig. 2). Although 1–99mRunx+m $E_{gre}$  was the only virus with significantly extended tumor latency

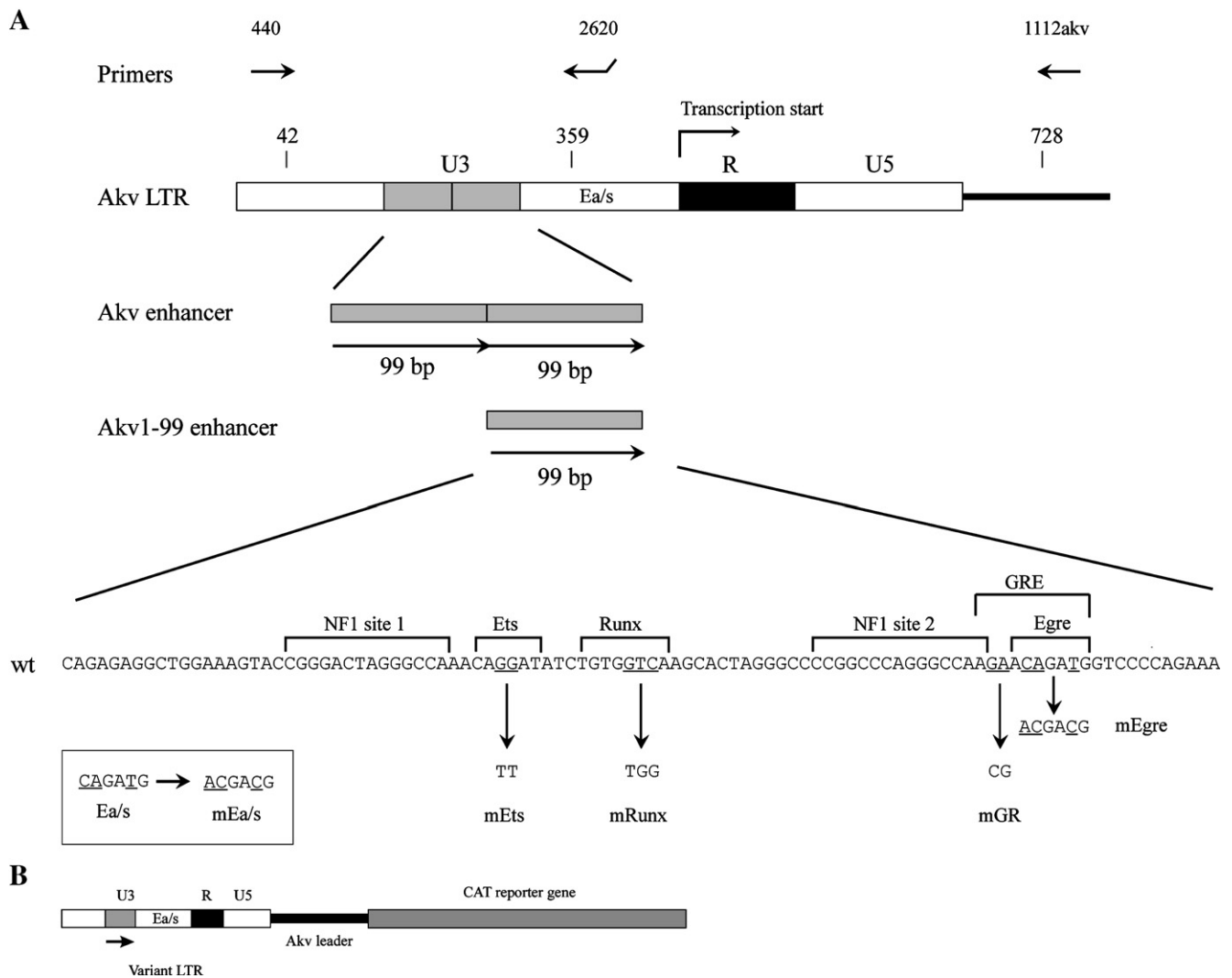


Fig. 1. (A) Proviral enhancer structures of Akv and Akv1–99 MLV. Akv contains two direct copies of a 99-bp enhancer sequence, whereas one copy has been deleted in the U3 region of Akv1–99. The complete 99-bp nucleotide sequence with indications of binding site motifs for cellular transcription factors is also given: NF1 (nuclear factor 1), Ets, Runx (core), GRE (glucocorticoid response element) and  $E_{gre}$  (E-box, bHLH/basic helix–loop–helix site). An additional E-box site ( $E_{a/s}$ ) is present in the U3 region downstream of the enhancer. Specific point mutations used to generate nine different Akv1–99 transcription control mutants (1–99mEts, 1–99mRunx, 1–99mGR, 1–99m $E_{gre}$ , 1–99m $E_{a/s}$ , 1–99mRunx+mGR, 1–99mGR+m $E_{gre}$ , 1–99mGR+m $E_{a/s}$  and 1–99m $E_{gre}$ +m $E_{a/s}$ ) are indicated at the bottom. The Ets core consensus binding sequence (GGAA/T (Sementchenko and Watson, 2000)) was disrupted by a GG to TT substitution, originally used by others to mutate the equivalent site (LVb) in MoMLV (Speck et al., 1990). The 3-bp TGG Runx site mutation abolishes DNA–protein complex formation in vitro (Thornell et al., 1988, 1991), as exploited in previous studies of SL3-3 MLV (Ethelberg et al., 1997b; Hallberg et al., 1991; Sørensen et al., 2004). A 1-bp change  $CAGATG$  to  $AAGATG$  in  $E_{gre}$  eliminates in vitro binding of class A bHLH factors, transactivation in vivo and dexamethasone-induced activation via glucocorticoid receptor (GR) binding to GRE (Nielsen et al., 1994, 1996), however, two additional alterations were introduced into  $E_{gre}$  and  $E_{a/s}$  ( $CAGATG$  to  $ACGACG$ ) in this study to avoid reversion in vivo by a single point mutation. The  $E_{gre}$  site mutation also interrupts GRE (consensus sequence:  $AGAACA(N)_3TGTCT$  (Beato et al., 1995)), while the GA to CG mutation in GRE is positioned upstream of the  $E_{gre}$  site consensus sequence (E-box:  $CANNTG$  (Massari and Murre, 2000)). Primers used for PCR amplification of proviral U3 regions are shown at the top. (B) Outline of the chloramphenicol acetyltransferase (CAT) reporter construct used. CAT expression is driven by a complete proviral LTR, which in the example shown has the structure of Akv1–99.

compared to Akv1–99, all double mutants induced tumors with shorter mean latency than their corresponding single site mutants (significant in all cases, except 1–99 mRunx+mGR) (Table 2). The present findings for Akv/Akv1–99, with none of the mutations having a major influence on mean tumor latencies, contrast the highly debilitating effects on viral oncogenicity reported for certain enhancer mutants of closely related T-lymphomagenic viruses SL3-3 and MoMLV (Ethelberg et al., 1997b; Hallberg et al., 1991; Morrison et al., 1995; Nieves et al., 1997; Speck et al., 1990; Sørensen et al., 2004).

We note that small differences in tumor induction may be hidden by the short mean latencies measured in inbred NMRI mice.

#### *Preservation of point mutations in proviral U3 regions amplified from genomic tumor DNA*

The effect on viral pathogenicity of introduced point mutations can be counteracted by reversion or suppressor mutations arising during tumor induction in vivo. To test this

Table 1  
Transient transfection assays with CAT reporter constructs

Enhancer variant	Relative CAT activity (SD) <sup>a</sup>			
	MPC11	NALM6	L691	NIH 3T3
Akv1–99	100	100	100	100
1–99 mEts	37 (18)	22 (2)	25 (8)	19 (5)
1–99 mRunx	37 (13)	28 (1)	28 (5)	19 (15)
1–99 mGR	49 (6)	68 (3)	30 (1)	56 (15)
1–99 mE <sub>gre</sub>	51 (5)	32 (5)	25 (2)	31 (13)
1–99 mE <sub>a/s</sub>	40 (3)	44 (7)	35*	26 (3)
1–99 mRunx+mGR	35 (14)	34 (8)	44*	25 (2)
1–99 mRunx+mE <sub>gre</sub>	8 (6)	10 (1)	40*	5 (2)
1–99 mGR+mE <sub>a/s</sub>	ND	ND	ND	24 (14)
1–99 mE <sub>gre</sub> +mE <sub>a/s</sub>	14 (6)	10 (1)	44*	7 (1)

<sup>a</sup> Average CAT activities were normalized to the activity of pAkvl–99cat, which was arbitrarily set to 100. Standard deviations of 2–8 independent transfections, all performed in duplicate, are given. A few transfections were performed only once and are marked by asterisks. ND, not determined.

possibility, proviral U3 regions were PCR amplified in bulk from genomic tumor DNA samples from 198 mice, equally representing all viruses. In most cases (mice infected with Akv, Akvl–99 and Akvl–99 mutants with an intact E<sub>a/s</sub> site), proviral U3 sequences were amplified with a primer (440) in the 5' end of the U3 region and a primer (2620) located ca. 60 bp downstream of the enhancer (i.e. overlapping the E<sub>a/s</sub> site) (Fig. 1A). Amplification products were sequenced from position 42 to 260/359 (Akv1–99/Akv) of the proviral LTR. In cases having the E<sub>a/s</sub> site mutated (1–99mE<sub>a/s</sub>, 1–99mGR+mE<sub>a/s</sub> and 1–99mE<sub>gre</sub>+mE<sub>a/s</sub>), primer 440 was used instead with a primer

(1112akv) in the 5' UTR (Fig. 1A). Nucleotide sequences of the resulting amplicons were determined from position 42 to the end of the U3 region (nt 383, Akvl–99). The two primer sets did not amplify endogenous sequences from non-infected control mice (data not shown).

Samples from Akv-induced tumors consistently (22 out of 22 tumors) produced two bands of the respective sizes predicted for Akv with two copies of the 99-bp enhancer (376 bp) or with one complete 99-bp repeat deleted (277 bp) (data not shown), as we later verified by sequencing. DNA samples from wildtype and mutant Akvl–99-induced tumors gave only a single PCR band (176 of 176 tumors) corresponding to the size expected for a one-copy 99-bp enhancer containing virus (277 bp/644 bp dependent on primer usage) (data not shown). Sequencing of the amplified proviral U3 regions showed that the introduced point mutations were maintained in all cases. Akv and Akvl–99 virus sequences also had not changed and no second-site mutations were detected. Repeat gain(s) were not observed in any of the 198 cases. The consistent conservation of point mutations in the Ets, Runx, E<sub>gre</sub>, GRE and E<sub>a/s</sub> motifs in proviruses from tumor DNA correlates well with the moderate effects of these mutations on viral tumor latency periods (Table 2).

#### Distinct disease induction patterns of Akv and Akvl–99

Histopathological examination revealed marked phenotypic differences in tumor induction by Akv and Akvl–99 in inbred NMRI. Akv induced three main tumor types: 35% plasma cell proliferations, 33% diffuse large B-cell lymphoma (DLBCL)

Table 2  
Tumor induction in inbred NMRI mice

Virus	Tumor incidence <sup>a</sup>		Mean tumor latency in days (SD)	DNA rearrangements <sup>b</sup>				Incidence of clonal B-cell lymphoma <sup>c</sup>
				Igκ	IgH	TCRβ-J1	TCRβ-J2	
Akv	40/40	(100%)	184 (26)	7/26	7/20	0/27	0/26	9/27 (33%)
Akv1–99	49/50	(98%)	180 (23)	9/33	4/22	1/32	1/22	11/35 (31%)
1–99 mEts	43/44	(98%)	182 (27)	8/16	5/11	0/17	1/16 <sup>d</sup>	9/16 (56%)
1–99 mRunx	37/39	(95%)	149 (22) <sup>e</sup>	2/22	2/17	0/10	0/19	4/22 (18%)
1–99 mGR	40/41	(98%)	145 (28) <sup>e</sup>	5/23	1/9	0/9	1/22 <sup>f</sup>	5/23 (22%)
1–99 mE <sub>gre</sub>	41/42	(98%)	160 (27) <sup>e</sup>	5/20	4/19	0/6	0/22	7/20 (35%)
1–99 mE <sub>a/s</sub>	47/47	(100%)	165 (23) <sup>e</sup>	7/19	5/10 <sup>g</sup>	1/18 <sup>g</sup>	1/22 <sup>g</sup>	7/19 (37%)
1–99 mRunx+mGR	47/48	(98%)	160 (29) <sup>e</sup>	4/10	4/10	0/10	0/10	4/10 (40%)
1–99 mRunx+mE <sub>gre</sub>	45/46	(98%)	199 (35) <sup>e,h</sup>	6/14	nd	0/17	3/20 <sup>i</sup>	6/14 (43%)
1–99 mGR+mE <sub>a/s</sub>	46/49	(94%)	186 (26) <sup>h</sup>	3/10	2/10	0/10	0/10	3/10 (30%)
1–99 mE <sub>gre</sub> +mE <sub>a/s</sub>	41/41	(100%)	183 (38) <sup>h</sup>	4/10	3/10	0/10	0/10	4/10 (40%)
Mock <sup>j</sup>	1/29	(3%)	–	–	–	–	–	–

<sup>a</sup> Number of mice with tumor development (diagnosed on the basis of significantly enlarged lymphoid organs)/number of mice injected (percentage).

<sup>b</sup> As determined by Southern blotting analysis using T-cell receptor β, immunoglobulin heavy and kappa light chain gene specific hybridization probes (number of tumors with clonal rearrangements/number of tumors investigated). nd, not determined.

<sup>c</sup> As defined by the detection of clonal IgH and/or Igκ rearrangements by Southern analysis of genomic tumor DNA. In some cases, data were available for only one of the Ig loci.

<sup>d</sup> This tumor also had IgH and Igκ clonally rearranged, but was not further analyzed.

<sup>e</sup> Significantly different from Akvl–99 ( $p < 0.05$ ; log-rank test).

<sup>f</sup> One thymic tumor developed relatively fast (107 days) and had TCRβ-J2 but not Igκ clonally rearranged, indicating a T-lineage origin. Histopathological examination was not performed in this case.

<sup>g</sup> One thymic tumor had TCRβ-J1, -J2 and IgH, but not Igκ clonally rearranged. It was histologically diagnosed as a pre-T-cell lymphoblastic lymphoma.

<sup>h</sup> Significantly different from both of the corresponding single site mutants ( $p < 0.05$ ; log-rank test).

<sup>i</sup> These cases also had clonal Igκ but not TCRβ-J1 rearrangements.

<sup>j</sup> Two control groups, C1 and C2, with 15 and 14 mice, respectively, were combined. They were sacrificed at 246 (C1) and 300 (C2) days of age. In group C1 enlargement of the spleen and mediastinal lymph nodes, indicative of lymphoma, was observed in one mouse at day 246.

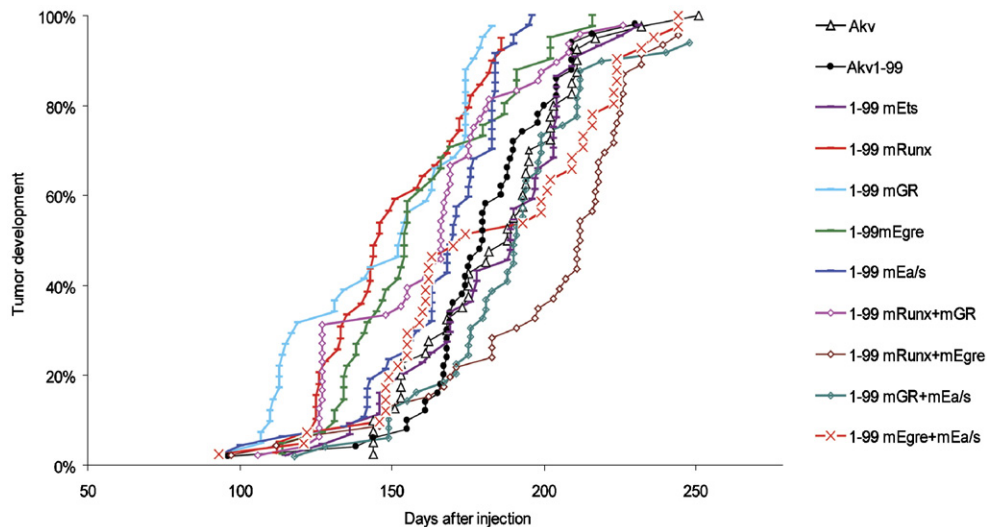


Fig. 2. Pathogenicity in inbred NMRI mice. The curves show cumulative incidences of tumor development versus the number of days after injection of infectious virus particles into newborn mice.

and 23% follicular B-cell lymphoma (FBL). A few cases of splenic marginal zone lymphoma (SMZL) and small B-cell lymphoma (SBL) were also seen (Table 3). In this study, as well as in our previous work (Sørensen et al., 2005), the term plasma cell proliferation (PCP) refers to a histopathologically homogeneous disease entity, which at the molecular level represented a continuum ranging from polyclonal plasma cell proliferation to oligo-/monoclonal malignant plasma cell lymphoma, i.e. plasmacytoma (see below).

Although Akv1–99 retained the capacity to induce multiple B-cell tumor types, disease induction was strongly shifted towards PCP (77%) (Table 3). This shift was also highlighted by the finding of mixed tumors (PCP plus DLBCL, FBL, SMZL or SBL) in seven Akv1–99 infected mice (Table 3). Akv1–99 induced DLBCL in 19% of the mice in the present work, but only plasma cell proliferations (including plasmacytomas) were observed in our previous study (Sørensen et al., 2005). This discrepancy might be explained by the lower number of tumors examined histopathologically in the former work (Sørensen et al., 2005). One mouse infected with Akv1–99 developed a pre-T-cell lymphoblastic lymphoma. Thymus, spleen, cervical and mesenteric lymph nodes were markedly enlarged and diffusely infiltrated by a monotonous population of CD3 and TdT positive blastic cells (data not shown).

Infiltrated lymph nodes in mice with PCP showed partial effacement of the architecture with the presence of hyperplastic germinal centers lacking the mantle zone (so-called “naked” germinal centers), surrounded by a diffuse proliferation of medium-sized plasma cells with a monotonous appearance. In a few cases, the thymus was also infiltrated (Figs. 3A–C). Immunohistochemically, the plasma cells were CD79acy and CD138 positive (Fig. 3D, and data not shown). The proliferation rate was generally low, as judged from Ki-67 staining (data not shown). Plasma cell infiltration in the spleen was found primarily around the white pulp and in the red pulp, and in severe cases, naked germinal centers were also found (data not

shown). About 70% of the Akv- and 25% of the Akv1–99-induced PCPs contained mature plasma cells intermingled with large B cells or centroblasts (Figs. 3E–F), which stained positive for B220/CD45R, but not for CD138 (Fig. 3G, and data not shown). This tumor phenotype, which we refer to as PCP with large cell components (LCC) (Table 3), has not previously been described in mice. It showed marked morphological similarity to polymorphic post-transplant lymphoproliferative disorders in man, which are known to be antigen-driven (Jaffe et al., 2001; Lacasce, 2006). Hence, these cases may represent tumor progression. Southern analysis revealed no difference in Ig clonality between PCPs with and without LCC (Table 3).

DLBCLs were characterized by a diffuse infiltration of large blastic cells (Figs. 3H–I), predominantly in the white pulp of the spleen (data not shown). Partial involvement of the lymph nodes was observed in some cases (Figs. 3G–H). The liver was infiltrated in all cases (mainly in the portal areas) by nodules composed primarily of B220/CD45R and CD79acy positive large blastic cells, intermingled with reactive lymphocytes, granulocytes, eosinophils and histiocytes (Fig. 3J, and data not shown). In FBLs, the neoplastic cells stained positive for B220/CD45R and CD79acy and infiltrated the lymph nodes in a diffuse pattern, and less frequently the spleen. The neoplastic population was composed of a mixed population of centroblasts and centrocytes (Fig. 3K). The proliferation rate was high, as shown by Ki-67 staining (Fig. 5L).

Mice with SMZL showed severe splenomegaly. In all cases, the lymphoma was confined to the spleen. The red pulp was infiltrated by a monotonous population of medium-sized cells with abundant pale cytoplasm, central nucleus and fine chromatin. The phenotype of SMZL was unique in that the neoplastic cells were positive for CD79acy and in most cases negative for B220/CD45R (not shown). SBL was associated with splenomegaly and diffuse infiltration of lymphoid and non-lymphoid tissues by small, CD79acy positive B cells with scant

Table 3  
Histopathological characterization of virus-induced tumors

Virus	No. of mice examined by histopathology	Percent incidence of each tumor type (number of mice with a given tumor type/number of mice examined)										
		PCP w.o. LCC	PCP w. LCC	PCP w. LCC	PCP (total)	DLBCL	FBL	SMZL	SBL	ML	preT-LBL	
Akv	40	10% (4/40)	25% (10/40)	35% (14/40)	33% (13/40)	23% (9/40)	5% (2/40)	5% (2/40)	–	–	–	
Akv1–99	48	58% (28/48)	19% (9/48)	77% (37/48)	19% (9/48) <sup>a</sup>	6% (3/48) <sup>a</sup>	8% (4/48) <sup>b</sup>	2% (1/48)	–	–	2% (1/48)	
1–99 mEts	43	21% (9/43)	74% (32/43)	95% (41/43)	–	5% (2/43)	2% (1/43) <sup>b</sup>	–	–	–	–	
1–99 mRunx	10	100% (10/10)	–	100% (10/10)	–	–	–	–	–	–	–	
1–99 mGR	10	50% (5/10)	50% (5/10)	100% (10/10)	–	–	10% (1/10) <sup>b</sup>	–	–	–	–	
1–99 mE <sub>gre</sub>	10	70% (7/10)	30% (3/10)	100% (10/10)	–	–	–	–	20% (2/10) <sup>b</sup>	–	–	
1–99 mE <sub>a/s</sub>	46	37% (19/46)	57% (26/46)	98% (45/46)	–	–	7% (3/46) <sup>c</sup>	–	–	–	2% (1/46) <sup>b</sup>	
1–99 mRunx+mGR	10	90% (9/10)	10% (1/10)	100% (10/10)	–	–	–	–	–	–	–	
1–99 mRunx+mE <sub>gre</sub>	45	84% (38/45)	13% (6/45)	98% (44/45)	–	2% (1/45)	–	–	–	–	–	
1–99 mGR+mE <sub>a/s</sub>	10	70% (7/10)	30% (3/10)	100% (10/10)	–	–	10% (1/10) <sup>b</sup>	–	–	–	–	
1–99 mE <sub>gre</sub> +mE <sub>a/s</sub>	10 <sup>d</sup>	70% (7/10)	20% (2/10)	90% (9/10)	–	–	–	–	–	–	–	
Igκ and/or IgH clonally rearranged by Southern blotting analysis <sup>e</sup>	–	29/89 (33%)	20/51 (39%)	49/131 (37%)	5/18 (28%)	4/7 (57%)	3/6 (50%)	1/2 (50%)	0/1 (0%)	0/2 (0%)	0/2 (0%)	
Mean tumor latency (SD) <sup>e</sup>	–	176 (35)	184 (24)	178 (32)	191 (18)	178 (33)	177 (32)	158 (12)	141 (13)	115 (27)	–	

<sup>a</sup> One of these mice had PCP along with the indicated tumor type.

<sup>b</sup> All of these mice had PCP along with the indicated tumor type.

<sup>c</sup> Two of these mice had PCP along with the indicated tumor type.

<sup>d</sup> One mouse had follicular hyperplasia without signs of malignant disease (age 244 days, lacked clonal Igκ and IgH rearrangements by Southern analysis).

<sup>e</sup> Only mice with a histopathological diagnosis were included.

cytoplasm, condensed chromatin and inconspicuous nuclei (not shown).

In contrast to these clearly different disease induction patterns of Akv and Akv1–99 in inbred NMRI mice, our former work showed similar lymphomagenic properties of the two viruses in random-bred NMRI mice with predominant induction of DLBCLs and B-cell lymphoblastic lymphomas, and no plasmacytomas (Lovmand et al., 1998 and unpublished). Hence, different mechanisms of viral disease induction may exist in inbred and random-bred NMRI mice.

#### Restricted tumor induction by Akv1–99 mutants

The nine Akv1–99 mutants induced almost exclusively PCPs (90–100%) (Table 3). Notably, all of the mutants had lost the ability to induce DLBCL. Other tumor types, including FBL, SMZL, myeloid leukemia with maturation and pre-T-cell lymphoblastic lymphoma, were seen in some of the mutant series (1–99mEts, 1–99mGR, 1–99mE<sub>gre</sub>, 1–99mE<sub>a/s</sub>, 1–99mRunx+mGR, 1–99mRunx+mE<sub>gre</sub>, 1–99mGR+mE<sub>a/s</sub>), however, these cases were rare and mostly identified in mice also diagnosed with PCP (Table 3 and data not shown). In the three mice with myeloid leukemia, the spleen was infiltrated by more than 20% myeloblasts (positive for myeloperoxidase) and granulocytes in all maturation stages (not shown).

The ratio of PCP with or without LCC (Table 3) as well as the incidence of detectable clonal immunoglobulin rearrangements by Southern blotting analysis (Table 2 and see below) showed considerable variation between the nine mutant series. We found no simple correlation between these measures, but note that 1–99mEts-infected mice presented with both the highest fraction of PCP with LCC (32/41) and the highest incidence of clonal B-cell lymphoma (56%), whereas the lowest incidence of PCP with LCC (0/10) and clonal B-cell lymphoma (18%) was seen in 1–99mRunx-infected mice (Tables 2 and 3). Furthermore, the two double mutants with the Runx site mutated (1–99mRunx+mGR and 1–99mRunx+mE<sub>gre</sub>) induced the second and third lowest incidences of PCP with LCC (Table 3), altogether suggesting that out of the five binding sites investigated, the Runx site contributes most strongly and the Ets site most weakly to Akv1–99 oncogenic potency. A comparison of the phenotypic disease patterns induced by all Akv viruses in this study (Table 3) suggests that viral enhancer strength is important for induction of the mature B-lymphoma types DLBCL and FBL, while this is not needed for induction of plasma cell proliferations.

#### Molecular tumor analysis

For further characterization, Southern blotting analysis of genomic tumor DNA was performed using hybridization probes specific for the immunoglobulin kappa light chain (Igκ), the immunoglobulin heavy chain (IgH) and the T-cell receptor β (TCRβ) loci (Fig. 4). Clonal TCRβ rearrangements were detected in only a few samples (7 out of 199) (Table 2; Figs. 4A, C), consistent with the histological finding of mainly B-cell

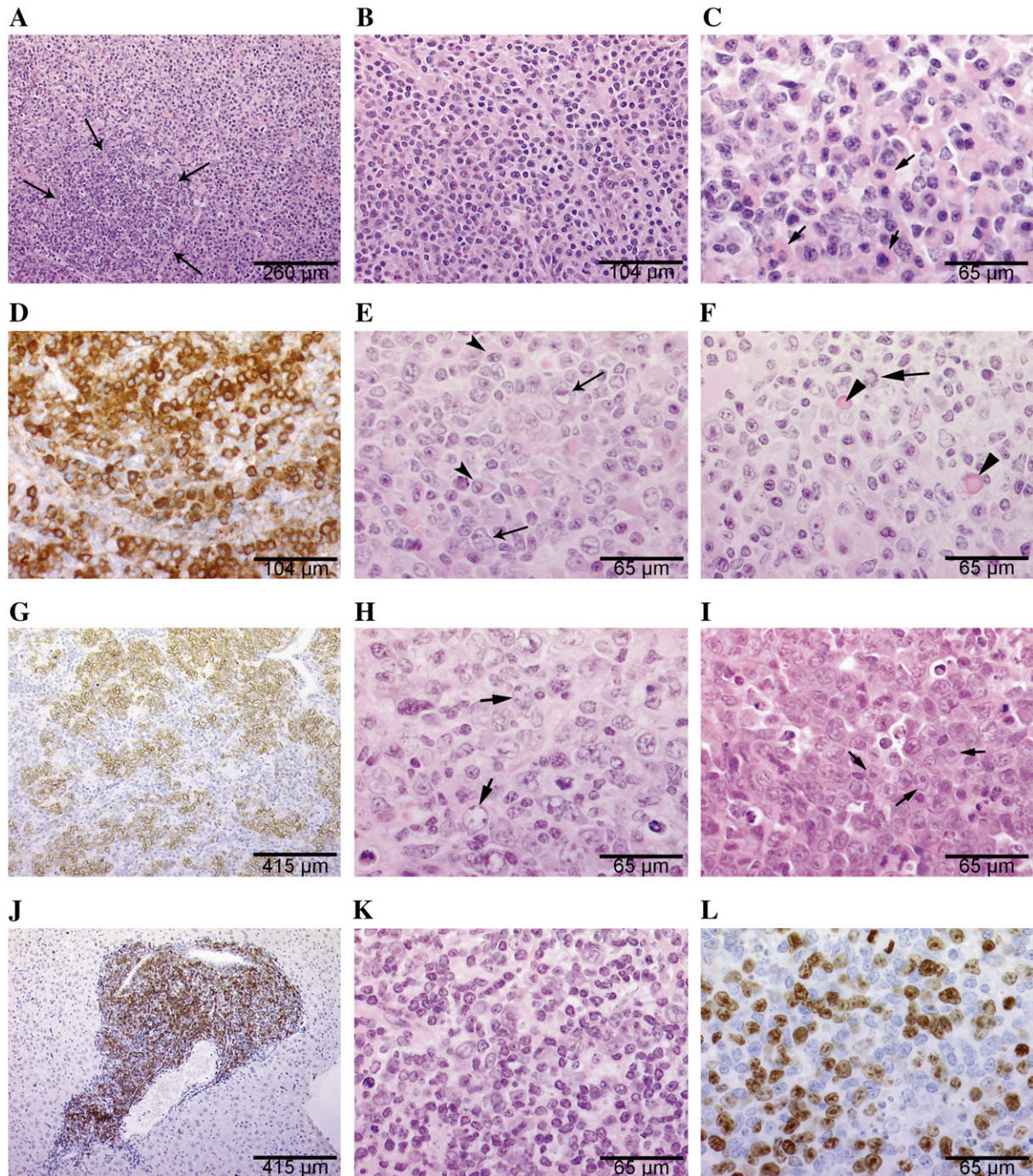


Fig. 3. Histopathological and immunohistological analysis of tumor tissues. Enlarged lymph nodes, spleen and thymus from retrovirus-infected inbred NMRI mice. (A–D) Plasma cell proliferation. (A) Section of thymus showing a monotonous proliferation of plasma cells surrounding a “naked” germinal center (indicated by arrows) (H&E). (B) Lymph node with a monotonous proliferation of medium-sized plasma cells with abundant cytoplasm. (C) A higher magnification demonstrates the presence of abundant Russell bodies (arrows), which are plasma cells with abundant immunoglobulins in the cytoplasm (H&E). (D) Plasma cells are positive for CD79acy (IHC, lymph node). (E–F) Plasma cell proliferation with a large cell component. (E) Lymph node infiltrated with a mixture of medium-sized plasma cells (short arrow) and larger lymphoid cells (large arrow), which have irregular nuclei, blastic chromatin, one to three eosinophilic nucleoli and abundant pale cytoplasm (H&E). (F) Another field reveals the presence of mitotic figures (large arrow) and Russell bodies (short arrows) (H&E). (G–J) Diffuse large B-cell lymphoma (DLBCL). (G) Lymph node partially infiltrated by a B-cell lymphoma. Note that the tumor cells are B220 positive (IHC). (H) Lymph node diffusely infiltrated by large centroblastic cells with blastic chromatin and prominent nucleoli (arrows) (H&E). (I) Spleen infiltrated by large lymphoid cells with blastic chromatin, one big central nucleolus and abundant cytoplasm characteristic of immunoblastic lymphoma (H&E). (J) Liver infiltrated by a DLBCL positive for B220 (IHC). (K–L) Lymph node with murine follicular B-cell lymphoma. (K) The tumor population is composed of small and large cleaved and non-cleaved germinal center cells (H&E). (L) Note the high proliferation rate of the tumor demonstrated with the proliferation marker Ki-67 (IHC).

tumor induction. Three mice infected with Akv1–99 (Fig. 4A, lane 5), 1–99mGR or 1–99mE<sub>a/s</sub> had TCR $\beta$  but not Ig $\kappa$  clonally rearranged (Table 2). Histologically, two of these were pre-T-cell lymphoblastic lymphomas, one was not analyzed (1–99mGR). Four mice (one infected with 1–99mEts, three with 1–99mRunx+mE<sub>gre</sub>) had TCR $\beta$  and Ig $\kappa$  clonally rearranged (Table 2). These cases were histologically diagnosed as plasma cell proliferations.

One third of the mice infected with Akv or Akv1–99 had detectable Ig rearrangements, whereas the incidence varied from 18% to 56% in the mutant-infected mice (Table 2; Figs.

4A, C). No consistent correlation was seen by comparing single site to matching double site mutated viruses, raising the possibility that some of the variation may be stochastic. In some cases, clonal rearrangements were detected by Southern analysis in only one of the Ig loci. There was no morphological evidence for a pre-B-cell lymphoma in the tumors having IgH but not Ig $\kappa$  clonally rearranged.

Hybridization with an ecotropic env gene-specific probe to Southern blots of tumor DNA digested with *Hind*III (no cutting sites in Akv/Akv1–99) gave a smear rather than distinct band(s) in the vast majority of cases (Figs. 4A, C–

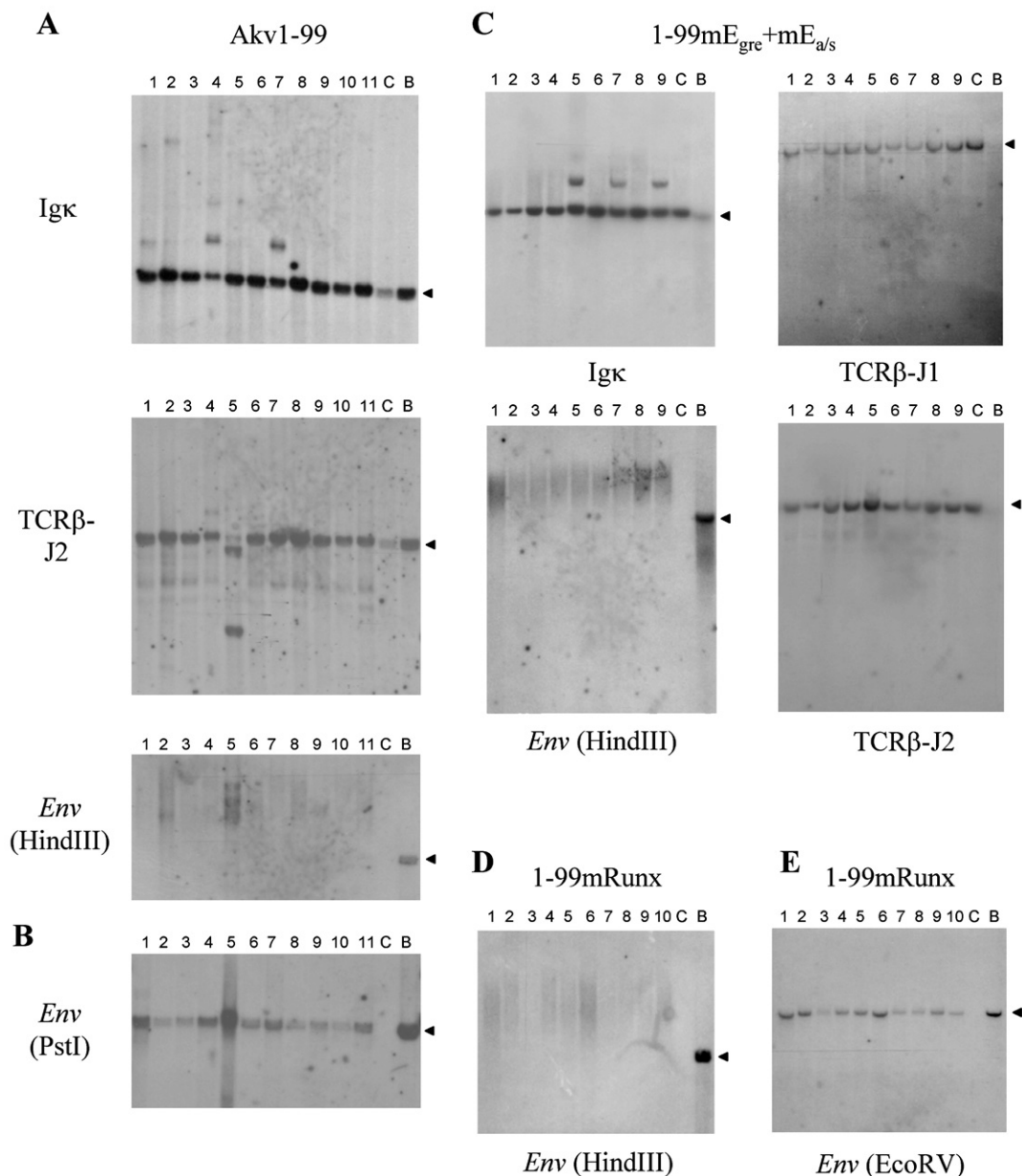


Fig. 4. Southern blotting analysis of virus-induced tumors. Representative results obtained from tumors induced by Akv1–99 (A–B), 1–99mE<sub>gre</sub>+mE<sub>a/s</sub> (C) and 1–99mRunx (D–E). Genomic tumor DNA samples were cut with *Hind*III (A, C, D), *Pst*I (B) or *Eco*RV (E), transferred to nylon membranes and hybridized with Ig $\kappa$ , TCR $\beta$ -J1, TCR $\beta$ -J2 or ecotropic *env* gene-specific probe as indicated. Numbers above each lane indicate individual tumors analyzed for each virus; lane C, control DNA from non-infected inbred NMRI mice; lane B, genomic liver DNA from Balb/c mouse harboring one endogenous ecotropic provirus. Germline bands are marked by arrow heads. One Akv1–99-induced tumor (A, lane 5), histologically diagnosed as a pre-B-cell lymphoma, had TCR- $\beta$  but not Ig $\kappa$  clonally rearranged. Detection of two distinct bands with the *env* hybridization probe indicated the presence of two clonal ecotropic provirus integrations in this tumor (A, bottom panel, lane 5).

D; and data not shown), indicating that most of the virus-induced tumors in inbred NMRI are oligo- or polyclonal with respect to provirus integrations. The low incidences of clonal Ig rearrangements (Table 3) may therefore be due to low tumor clonality. The presence of integrated ecotropic proviruses in the tumors was demonstrated by Southern hybridization to an approximately 8-kb internal env-containing provirus fragment generated by *Pst*I or *Eco*RV digestion of genomic tumor DNA (Figs. 4B, E). Finally, we note that the phenotypic disease patterns of all viruses (Table 3) were the same if only the cases with detectable clonal Ig rearrangements were included in the comparison (data not shown).

## Discussion

In the present study, we have undertaken a systematic analysis of disease induction by exogenous Akv, Akv1–99 and additional enhancer mutants. To address the role of the transcriptional enhancer, we chose to mutate sites of the enhancer framework associated with disease induction by T-lymphomagenic viruses, including binding sites for factors of the Runx and Ets families as well as E-box motifs and a GRE site overlapping one of the E-box motifs (Speck et al., 1990; Zaiman and Lenz, 1996; Zaiman et al., 1998). The mutations in all cases reduced viral enhancer strength in the lymphoid and fibroblast cell lines used for transient expression analysis. To unveil possible differences in induction of multiple diseases between the viruses, we used larger animal cohorts than in our previous studies (Lovmand et al., 1998; Sørensen et al., 2005). As discussed below, the main results of the present work are: (1) all viruses induce tumors of the B-cell lineage, (2) many tumors of all groups are polyclonal and (3) enhancer mutations inhibit induction of mature B-cell lymphomas (DLBCL and FBL) and shift tumor induction towards the fully differentiated plasma cell stage.

Using inbred NMRI mice, we found that Akv, Akv1–99 and all Akv1–99 enhancer mutants induced lymphomas or other lymphoproliferative diseases in the B-cell compartment with nearly 100% incidence and mean latencies of 5 to 7 months. For all viruses, clonal or oligoclonal B-cell expansions were detected in some but not all animals by Southern analysis of immunoglobulin rearrangements. This Southern pattern resembles that previously observed for Akv1–99 and Akv1–99 NF1 site mutants in this mouse strain (Sørensen et al., 2005). Moreover, several independent tumors of the present study displayed rearranged Ig fragments of similar sizes (Fig. 4, and not shown), as also noted in our former work on wildtype and NF1 site mutated Akv1–99 (Sørensen et al., 2005). This is, however, clearly distinct from the prominent Ig rearrangement patterns with bands of diverse sizes reported for both Akv and Akv1–99-induced tumors in random-bred NMRI mice (Lovmand et al., 1998). Although co-migration of fragments does not prove identity, it may suggest that the repertoire of Ig rearrangements is restricted in the B-cell tumors of inbred NMRI mice, irrespectively of the virus mutant used.

These observations extend our previous suggestion that B-cell lymphoma induction by Akv viruses in the inbred NMRI mouse strain may involve an immunostimulatory component (Sørensen et al., 2005). Such stimulation may cause a polyclonal expansion of B cells early during infection as well as chronic antigen-specific stimulation of individual clones at later stages of the disease. Although the animals are infected just after birth to avoid a neutralizing immune response, it is conceivable that this state of tolerance involves signaling in the innate and specific immune response (Sarzotti et al., 1996). For example, it is now recognized that retroviruses may activate several members of the toll-like receptor family (Heil et al., 2004; Rassa et al., 2002). Immune stimulation of newborn mice may be a distinguishing feature from models of spontaneous B-lymphoma development following the activation of endogenous retroviruses. In support of this possibility, we recently reported that the interferon response gene *Icsbp/Irf8*, which has never been identified as a common insertion site in spontaneous B-lymphomas, is a common insertion site in the models reported in the present manuscript (Ma et al., 2006).

Because of the cohort sizes, even small differences in latency periods among the mutants could be determined as significant in some cases, whereas the latency periods to disease induction by Akv and Akv1–99 were indistinguishable. Some enhancer mutants with alterations of a single transcription factor motif (1–99mRunx, 1–99mGR, 1–99mE<sub>gre</sub>, 1–99mE<sub>a/s</sub>) or two motifs (1–99mRunx+mGR) induced disease with slightly shorter latency periods than their parental Akv1–99 virus. We have no good explanation for this, but note that mutants with alterations in two motifs were associated with slightly longer latency periods than their corresponding single site mutants. Except for the frequent deletion of one of the two 99-bp enhancer copies in Akv-induced tumors, all viral enhancer sequences were stably maintained in vivo, reflecting that there is no strong selection for reversion or second-site alterations towards more rapid tumor development. Such changes have been extensively found in T-lymphomagenic viruses with disease-attenuating enhancer mutations of e.g. the Runx site (Ethelberg et al., 1997a; Martiney et al., 1999; Morrison et al., 1995; Sørensen et al., 2004). Hence, our present findings support the notion that key sites of the enhancer are not critical for the latency to disease induction in the Akv-based tumor models. Likewise, in our previous work, we found that mutation of one or both NF1 sites in Akv1–99 had no effect on latency to disease induction (Sørensen et al., 2005).

Interestingly, mutations of the proviral enhancer caused a shift in disease specificity independent of the latency periods to disease induction. Akv induced about equal incidences of the three major classes of tumors, FBLs at the germinal center stage, DLBCLs at the more mature post-germinal center stage and tumors of the fully mature plasma cell stage, plus a few cases of tumors of other stages (splenic marginal zone lymphomas and small B-cell lymphomas). For Akv1–99, which lacks the duplication of the 99-bp enhancer, the pattern of disease induction was shifted to few FBLs, 19% DLBCLs and 77% plasma cell proliferations. This shift was even more

pronounced for all of the enhancer mutants, where plasma cell proliferations constituted 95–100% of all cases. These findings indicate that the preferential induction of mature B-cell tumor types (particularly DLBCL and FBL) prior to the plasma cell stage requires an intact Akv enhancer. Our results may further suggest that the development of plasma cell proliferations (plasmacytomas) is less dependent or independent of viral enhancer strength, or possibly even favored by a weakened enhancer. Consistent with this, we have previously found that Akv1–99 transient enhancer activity is more than 2-fold lower than that of wildtype Akv in an early B-cell line (NALM6), whereas deletion of one 99-bp enhancer repeat has no effect on enhancer activity in fully differentiated MPC11 plasmacytoma cells (Lovmand et al., 1998; Sørensen et al., 2005).

Although the overall disease patterns induced by the enhancer mutants in inbred NMRI were very similar, minor differences in the presence or absence of LCCs and in the frequency of detectable Ig rearrangements suggested that the Runx site contributes the most and the Ets site the least to Akv1–99 pathogenic potency. We note that transient enhancer activities of 1–99mEts and 1–99mRunx were very similar in all four cell lines tested (Table 1), despite the small difference in disease induction patterns. The most likely explanation for this is the usage of only a limited number of representative cell lines in this study. The cell lines may not truly reflect the target cell type(s) of viral infection in vivo during a complex multi-step tumor induction process. Retrospectively, due to its broader disease specificity in inbred NMRI mice, it is likely that Akv would have provided a better background than Akv1–99 for read-outs of possible differential effects of individual binding site mutations.

The transcriptional enhancer may exert its role in the specificity of disease induction through an effect on viral

expression and/or replication in a given tissue, through its ability to deregulate the expression of host genes by insertional mutagenesis, or by a combination of the two. We know that insertional mutagenesis is involved in disease induction by exogenous Akv-type viruses since common insertion sites have been identified in tumors of random-bred (Martin-Hernandez et al., 2001; Martin-Hernandez et al., 2006) and inbred NMRI mice (Ma et al., 2006, and unpublished). We recently reported that Akv and Akv1–99 proviruses in tumors differed by their overall positions relative to host transcription units (Martin-Hernandez et al., 2006), suggesting that the proviral enhancer influences the specific pattern of insertional mutagenesis in a given tumor model. One interesting possibility is that the unimpaired Akv enhancer is a more potent insertional activator of e.g. stage-specific transcription factor genes, which may serve to restrict differentiation along the B-cell lineage. The enhancer mutants may be weaker in such activation and function by a somewhat different register of insertional mutations that allow the normal differentiation path for activated B cells to plasma cells. In fact, the plasma cells in the tumors may be the progeny of less differentiated tumor stem cells (Wang and Dick, 2005). Further analysis of proviral insertions may help elucidate the potential influence of mutations that restrict differentiation.

Our interpretation of the combined contributions from immune stimulation and insertional mutagenesis is shown in Fig. 5. We propose that intraperitoneal injection of viral supernatant into newborn mice activates an innate and/or specific immune response that leads to a polyclonal expansion of early B cells. The inbred NMRI model used in the present work may be particularly rapid and often present with polyclonal tumors because the immunostimulatory component is strong in this strain. The stimulated cells may be a further

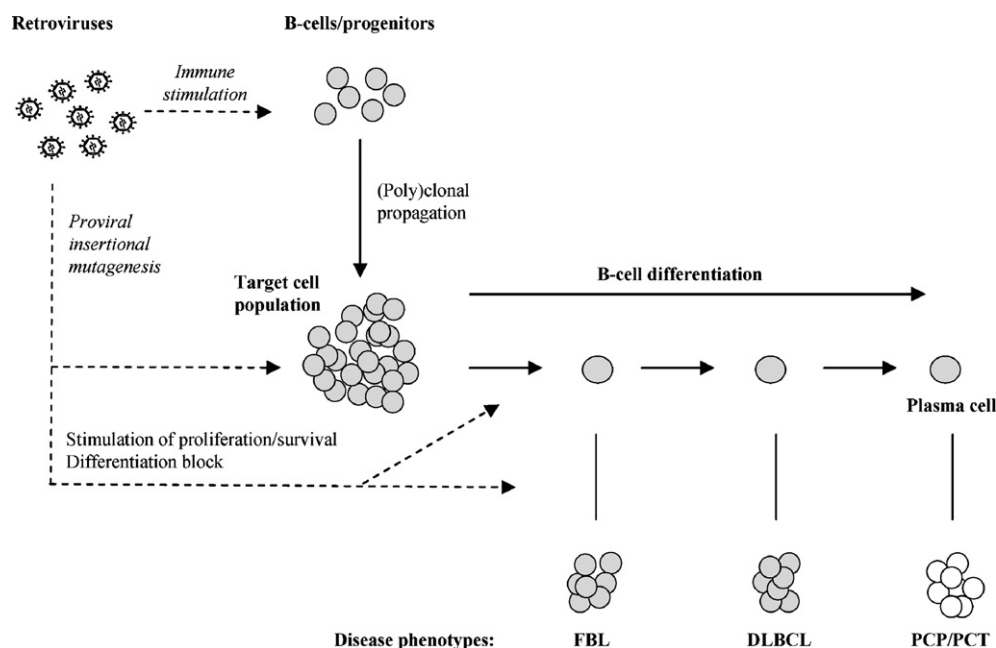


Fig. 5. Dual effects of immune-stimulatory events and insertional mutagenesis in wildtype and enhancer mutated Akv-induced disease in inbred NMRI mice. FBL, follicular B-cell lymphoma; DLBCL, diffuse large B-cell lymphoma; PCP, plasma cell proliferation; PCT, plasmacytoma. See text for further description.

target for viral infection, and proviral insertional mutagenesis at the progenitor or more mature stage may affect the proliferative ability or survival of the cells, as well as regulatory genes that control differentiation. Dual contributions from mutations that block differentiation and mutations that promote cell cycling and survival are well-known from human leukemias (Steffen et al., 2005). To explain the differences in disease specificity of wildtype and enhancer mutated viruses, we propose that the immunostimulatory and proliferative components may be similar for all viruses, while proviruses with an impaired enhancer may be less potent in activating host transcription factors or other stage-specific genes that block differentiation.

Using random-bred NMRI mice, we have previously found highly similar tumor induction patterns for Akv and Akv1–99 with predominant induction of mature B-cell lymphomas and no plasmacytomas (Lovmand et al., 1998). This suggests that different mechanisms of viral disease induction exist in the two NMRI strains. The absence of plasmacytoma induction by Akv and Akv1–99 in random-bred NMRI mice may be explained by lack of a strong immunostimulatory component in this strain, the lack of which may also favor induction of B-cell tumor types prior to the fully differentiated stage. A reduced contribution from an immunostimulatory component in the random-bred NMRI strain may also explain the longer latency period to disease induction as well as the appearance of clear clonal Ig rearrangements in tumors of this strain. Moreover, mouse strain specific integration site patterns of Akv and Akv1–99 may influence disease induction in random-bred versus inbred NMRI mice.

Finally, we note that the proposed model and the morphological spectrum of the virus-induced tumors in inbred NMRI mice are remarkably similar to those described for human post-transplant lymphoproliferative disorders. These lesions are characterized by an early antigen-driven, usually polyclonal, plasma cell proliferation, which may later become polymorphic (can be poly-, oligo- or monoclonal) and eventually progress to DLBCL or less often plasmacytoma (Jaffe et al., 2001; Lacasce, 2006). Accumulation of translocations or other types of mutations associated with progression of this disease in man may be functionally comparable to mutagenesis by provirus insertion in the murine models.

A superimposed activity of polyclonal stimulation and insertional mutagenesis has been found in other models of retrovirus-induced disease. The spleen focus-forming virus of the Friend complex stimulates proliferation of erythroblasts, which may be further subject to insertional mutagenesis by the Friend helper virus, causing mono- or oligoclonal erythroleukemia (Ben-David and Bernstein, 1991). Moreover, in an early step of Moloney MLV-induced lymphomagenesis, extramedullary hematopoiesis leads to increased progenitor cell populations of multiple lineages that are the targets of proviral insertional mutagenesis (Fan, 1997). In murine acquired immunodeficiency syndrome, a somewhat different model system, a defective MLV is known to induce a polyclonal B-cell expansion that in rare cases develop into oligoclonal B-lymphomas through proviral insertional mutagenesis (Huang et al., 1995). Hence, the overall outcome of a given MLV

oncogenesis model may depend on the proliferative capability of polyclonally stimulated cells as well as the outgrowth of individual transformed cell clones. Future work should investigate in more detail the mechanisms of Akv disease induction in the inbred NMRI mouse model, e.g. by using genetically modified mice with disabled immune response, as well as by examining in detail the contributions of viral infection, replication and gene expression at both early and later stages of disease development.

## Materials and methods

### Cell culture

The murine MPC11 plasmacytoma B-cell line, NALM6 human pre-B cells, L691 murine T-lymphoma cells and NIH 3T3 murine fibroblasts were grown as described earlier (Ethelberg et al., 1997a; Sørensen et al., 2005).

### Plasmids

The plasmids pAkv6-cat and pAkv1–99-cat contain the complete proviral LTR of Akv and Akv1–99, respectively, to drive expression of a chloramphenicol acetyl transferase (CAT) reporter gene (Lovmand et al., 1998). Mutations in individual transcription factor binding sites of the Akv1–99 LTR region in pAkv1–99-cat were introduced by PCR-based mutagenesis using a 2-step overlap extension procedure. Two partially overlapping Akv1–99 LTR fragments with specific point mutations were generated with primer P1(akv) (5'-CCAGC-TAACTGCAGTAACGCCATTT TGC-3') plus mutPrimerX-reverse and primer P2(akv)-reverse (5'-ATACACGGGTACCC-GG GCGACTCAGTCT-3') plus mutPrimerX-forward, respectively (all mutPrimerX sequences are available upon request). Next, these fragments were extended and PCR amplified using primers P1(akv) and P2(akv)-rev. Double mutants were generated using single site mutants as template for PCR-based mutagenesis. The mutated PCR products were cut with *PstI* and *KpnI* and cloned into pAkv6-cat, producing the mutant CAT expression vectors p1–99mEts-cat, p1–99mRunx-cat, p1–99mGR-cat, p1–99mE<sub>gre</sub>-cat, p1–99mE<sub>a/s</sub>-cat, p1–99mRunx + mGR-cat, p1–99mRunx + mE<sub>gre</sub>-cat, p1–99mGR + mE<sub>a/s</sub>-cat and p1–99mE<sub>gre</sub> + mE<sub>a/s</sub>-cat. The proviral clones of Akv and Akv1–99 contain the entire viral genome with only one LTR (Lovmand et al., 1998). Nine different Akv1–99 proviral plasmids with mutations in transcription factor binding motifs in the LTR region were generated by replacing a *PvuI*–*PvuI* fragment from the proviral clone of Akv with the equivalent *PvuI*–*PvuI* fragment from each of the mutated Akv1–99 CAT expression plasmids.

### Virus stocks and animal experiments

The generation of wildtype Akv and Akv1–99 virus stocks has been described earlier (Lovmand et al., 1998). Infectious mutant viruses were produced by transfecting NIH 3T3 cells with concatemeric *PstI*–*PstI* fragments from mutant Akv1–

99 proviral plasmids. In all cases, virus production was monitored by measuring reverse transcriptase activity in cell culture supernatants (Hallberg et al., 1991), and the integrity of proviral LTR regions with introduced point mutations verified by PCR and sequencing (see below). Infectious virus particles were injected intraperitoneally into newborn inbred NMRI mice, as earlier described in details (Sørensen et al., 2004). Control mice of the same colony were mock-injected with 0.1 mL complete medium. The animals were monitored 5 days per week for a 9-month observation period. Mice were sacrificed and autopsied when showing signs of illness or tumor development (mainly palpable splenomegaly and/or lymphadenopathy, and fatigue). Tumor development was diagnosed on the basis of grossly enlarged lymphoid organs after having reached the size described earlier, which is compatible with lymphoma (Schmidt et al., 1984). Lymphoid tumor tissues and the liver were dissected, stored frozen ( $-80^{\circ}\text{C}$ ) and/or fixed in formalin for further analysis. Statistical analysis was carried out using the log-rank test.

#### *Histopathological examination and immunohistochemical analysis*

Formalin-fixed, paraffin-embedded sections of lymph nodes, thymus, spleen and liver were stained with hematoxylin and eosin (H&E), and when indicated with Giemsa, or PAS. Tumors were classified according to the Bethesda proposals for classification of murine hematopoietic neoplasms (Kogan et al., 2002; Morse et al., 2002). Immunohistochemistry (IHC) was performed on an automated immunostainer (Ventana Medical System, Inc.; AZ, USA), according to the protocol provided by the company with minor modifications. After deparaffination and rehydration, the slides were placed in a microwave pressure cooker in 0.01 M citrate buffer (pH 6.0), containing 0.1% Tween-20 and heated in a microwave oven at maximum power for 30 min. After cooling in Tris-buffered saline, the sections were incubated with 3% goat or rabbit serum for 20 min. The antibody panel used included CD3, CD79 $\alpha$ , TdT (Dako, Germany), CD138, B220/CD45R (BD Bioscience, NJ, USA), Ki-67 and MPO (DCS, Germany). Appropriate positive controls were used to confirm the adequacy of the staining.

#### *Southern blotting hybridization and DNA probes*

Genomic DNA was purified from frozen tumor tissues using the DNeasy tissue kit (Qiagen). Southern blotting, hybridization procedures and DNA probes have been described in details previously (Lovmand et al., 1998; Sørensen et al., 2004). In brief, 15  $\mu\text{g}$  of *Hind*III digested genomic tumor DNA was separated on 0.8% agarose gels, blotted onto nylon membranes and hybridized with  $^{32}\text{P}$  random priming labeled probes specific for the immunoglobulin kappa (Ig $\kappa$ ) light chain gene, the immunoglobulin heavy (IgH) chain gene (probe named IgH-J $_{11}$ ) and the T-cell receptor  $\beta$ -J1 and -J2 (TCR $\beta$ -J1 and -J2) joining region genes. The IgH-J $_{11}$  probe was used also with *Eco*RI digested DNA. An ecotropic viral envelope (env) gene-specific

probe (Lovmand et al., 1998) was hybridized to genomic DNA digested with *Hind*III or *Eco*RI (no cutting sites in Akv/Akv1–99) or with *Pst*I or *Eco*RV (generate an internal env containing Akv/Akv1–99 provirus fragment).

#### *Transfection and reporter assays*

The DEAE-dextran method (Ethelberg et al., 1997a) was used to transfect MPC11, NALM6 and L691 cells, whereas NIH 3T3 cells were transfected by calcium phosphate-mediated precipitation (Ethelberg et al., 1997a). Each transfection included 2  $\mu\text{g}$ /3  $\mu\text{g}$ /4  $\mu\text{g}$  (NIH 3T3/NALM6/L691 and MPC11) CAT expression vector together with 1.5  $\mu\text{g}$ /2  $\mu\text{g}$  (NIH 3T3/NALM6, L691 and MPC11) pRSV-luc internal control plasmid to correct for different transfection efficiencies, and 8  $\mu\text{g}$ /10  $\mu\text{g}$ /11.5  $\mu\text{g}$  (NALM6/L691 and MPC11/NIH 3T3) pUC19 carrier DNA. All transfections were done in duplicate and repeated 2 to 8 times, unless stated otherwise. CAT and luciferase activities were measured in whole cell extracts prepared 48 h after transfection by repeated cycles of freeze/thawing (Ethelberg et al., 1997a).

#### *PCR and DNA sequencing*

Proviral U3 enhancer–promoter regions were PCR amplified from genomic tumor DNA samples using a primer (440, 5'-TTCATAAGGCTTAGCCAGCTAAC TGCAG-3') in the 5' end of the U3 region in combination either with a primer (2620; 5'-GAATTTCGATATCGATCCCCGGTCATCTGGG-3') located ca. 60 bp downstream of the enhancer, i.e. overlapping the Ea/s site, or in cases with this site mutated (1–99mE $_{a/s}$ , 1–99mGR+mE $_{a/s}$  and 1–99mE $_{gre}$ +mE $_{a/s}$ ) a primer located in the 5' untranslated region (1112akv; 5'-GTAGATGCCGGCACACACACACACGCA-3'). PCR products were analyzed by agarose gel electrophoresis, purified and sequenced, as described previously (Sørensen et al., 2005).

#### **Acknowledgments**

We thank Lone Højgaard, Angelika Appold, Katrin Reindl, Jaqueline Müller, Claudia Kloss, Nadine Kink and Elenore Samson for excellent technical assistance. This work was supported by grants from the Danish Cancer Society, the Novo Nordic Foundation, the Karen Elise Jensen Foundation and the Danish Natural Sciences and Medical Research Councils.

#### **References**

- Beato, M., Herrlich, P., Schutz, G., 1995. Steroid hormone receptors: many actors in search of a plot. *Cell* 83 (6), 851–857.
- Ben-David, Y., Bernstein, A., 1991. Friend virus-induced erythroleukemia and the multistage nature of cancer. *Cell* 66 (5), 831–834.
- Celander, D., Hsu, B.L., Haseltine, W.A., 1988. Regulatory elements within the murine leukemia virus enhancer regions mediate glucocorticoid responsiveness. *J. Virol.* 62 (4), 1314–1322.
- Ethelberg, S., Hallberg, B., Lovmand, J., Schmidt, J., Luz, A., Grundström, T., Pedersen, F.S., 1997a. Second-site proviral enhancer alterations in lymphomas induced by enhancer mutants of SL3-3 murine leukemia virus: negative effect of nuclear factor 1 binding site. *J. Virol.* 71 (2), 1196–1206.

- Ethelberg, S., Lovmand, J., Schmidt, J., Luz, A., Pedersen, F.S., 1997b. Increased lymphomagenicity and restored disease specificity of AML1 site (core) mutant SL3-3 murine leukemia virus by a second-site enhancer variant evolved in vivo. *J. Virol.* 71 (10), 7273–7280.
- Fan, H., 1997. Leukemogenesis by Moloney murine leukemia virus: a multistep process. *Trends Microbiol.* 5 (2), 74–82.
- Gilbert, D.J., Neumann, P.E., Taylor, B.A., Jenkins, N.A., Copeland, N.G., 1993. Susceptibility of AKXD recombinant inbred mouse strains to lymphomas. *J. Virol.* 67 (4), 2083–2090.
- Golemis, E.A., Speck, N.A., Hopkins, N., 1990. Alignment of U3 region sequences of mammalian type C viruses: identification of highly conserved motifs and implications for enhancer design. *J. Virol.* 64 (2), 534–542.
- Hallberg, B., Schmidt, J., Luz, A., Pedersen, F.S., Grundström, T., 1991. SL3-3 enhancer factor 1 transcriptional activators are required for tumor formation by SL3-3 murine leukemia virus. *J. Virol.* 65 (8), 4177–4181.
- Hartley, J.W., Chattopadhyay, S.K., Lander, M.R., Taddesse-Heath, L., Naghashfar, Z., Morse III, H.C., Fredrickson, T.N., 2000. Accelerated appearance of multiple B cell lymphoma types in NFS/N mice congenic for ecotropic murine leukemia viruses. *Lab. Invest.* 80 (2), 159–169.
- Heil, F., Hemmi, H., Hochrein, H., Ampenberger, F., Kirschning, C., Akira, S., Lipford, G., Wagner, H., Bauer, S., 2004. Species-specific recognition of single-stranded RNA via toll-like receptor 7 and 8. *Science* 303 (5663), 1526–1529.
- Huang, M., Takac, M., Kozak, C.A., Jolicoeur, P., 1995. The murine AIDS defective provirus acts as an insertional mutagen in its infected target B cells. *J. Virol.* 69 (7), 4069–4078.
- Jaffe, E.S., Harris, N.L., Stein, H., Vardiman, J.W. (Eds.), 2001. Pathology and Genetics of Tumours of Hematopoietic and Lymphoid Tissues. World Health Organization Classification of Tumours. Edited by P. Kleihues, and L.H. Sobin. IARC Press, Lyon.
- Kogan, S.C., Ward, J.M., Anver, M.R., Berman, J.J., Brayton, C., Cardiff, R.D., Carter, J.S., de Coronado, S., Downing, J.R., Fredrickson, T.N., Haines, D.C., Harris, A.W., Harris, N.L., Hiai, H., Jaffe, E.S., MacLennan, I.C., Pandolfi, P.P., Pattengale, P.K., Perkins, A.S., Simpson, R.M., Tuttle, M.S., Wong, J.F., Morse III, H.C., 2002. Bethesda proposals for classification of nonlymphoid hematopoietic neoplasms in mice. *Blood* 100 (1), 238–245.
- Lacasse, A.S., 2006. Post-transplant lymphoproliferative disorders. *Oncologist* 11 (6), 674–680.
- Lenz, J., Celander, D., Crowther, R.L., Patarca, R., Perkins, D.W., Haseltine, W.A., 1984. Determination of the leukaemogenicity of a murine retrovirus by sequences within the long terminal repeat. *Nature* 308 (5958), 467–470.
- Lovmand, J., Sørensen, A.B., Schmidt, J., Østergaard, M., Luz, A., Pedersen, F.S., 1998. B-Cell lymphoma induction by Akv murine leukemia viruses harboring one or both copies of the tandem repeat in the U3 enhancer. *J. Virol.* 72 (7), 5745–5756.
- Ma, S.L., Sørensen, A.B., Kunder, S., Sørensen, K.D., Quintanilla-Martinez, L., Morris, D.W., Schmidt, J., Pedersen, F.S., 2006. The Icsbp locus is a common proviral insertion site in mature B-cell lymphomas/plasmacytomas induced by exogenous murine leukemia virus. *Virology* 352 (2), 306–318.
- Martin-Hernandez, J., Sørensen, A.B., Pedersen, F.S., 2001. Murine leukemia virus proviral insertions between the N-ras and unr genes in B-cell lymphoma DNA affect the expression of N-ras only. *J. Virol.* 75 (23), 11907–11912.
- Martin-Hernandez, J., Balle Sørensen, A., Pedersen, F.S., 2006. Non-identical patterns of proviral insertions around host transcription units in lymphomas induced by different strains of murine leukemia virus. *Virology* 353 (1), 193–199.
- Martiney, M.J., Levy, L.S., Lenz, J., 1999. Suppressor mutations within the core binding factor (CBF/AML1) binding site of a T-cell lymphomagenic retrovirus. *J. Virol.* 73 (3), 2143–2152.
- Massari, M.E., Murre, C., 2000. Helix–loop–helix proteins: regulators of transcription in eucaryotic organisms. *Mol. Cell. Biol.* 20 (2), 429–440.
- Morrison, H.L., Soni, B., Lenz, J., 1995. Long terminal repeat enhancer core sequences in proviruses adjacent to *c-myc* in T-cell lymphomas induced by a murine retrovirus. *J. Virol.* 69 (1), 446–455.
- Morse III, H.C., Anver, M.R., Fredrickson, T.N., Haines, D.C., Harris, A.W., Harris, N.L., Jaffe, E.S., Kogan, S.C., MacLennan, I.C., Pattengale, P.K., Ward, J.M., 2002. Bethesda proposals for classification of lymphoid neoplasms in mice. *Blood* 100 (1), 246–258.
- Mucenski, M.L., Taylor, B.A., Jenkins, N.A., Copeland, N.G., 1986. AKXD recombinant inbred strains: models for studying the molecular genetic basis of murine lymphomas. *Mol. Cell. Biol.* 6 (12), 4236–4243.
- Nielsen, A.L., Pallisgaard, N., Pedersen, F.S., Jørgensen, P., 1994. Basic helix–loop–helix proteins in murine type C retrovirus transcriptional regulation. *J. Virol.* 68 (9), 5638–5647.
- Nielsen, A.L., Nørby, P.L., Pedersen, F.S., Jørgensen, P., 1996. Various modes of basic helix–loop–helix protein-mediated regulation of murine leukemia virus transcription in lymphoid cell lines. *J. Virol.* 70 (9), 5893–5901.
- Nieves, A., Levy, L.S., Lenz, J., 1997. Importance of a c-Myb binding site for lymphomagenesis by the retrovirus SL3-3. *J. Virol.* 71 (2), 1213–1219.
- Rassa, J.C., Meyers, J.L., Zhang, Y., Kudravalli, R., Ross, S.R., 2002. Murine retroviruses activate B cells via interaction with toll-like receptor 4. *Proc. Natl. Acad. Sci. U. S. A.* 99 (4), 2281–2286.
- Sarzotti, M., Robbins, D.S., Hoffman, P.M., 1996. Induction of protective CTL responses in newborn mice by a murine retrovirus. *Science* 271 (5256), 1726–1728.
- Schmidt, J., Erfle, V., Pedersen, F.S., Rohmer, H., Schetters, H., Marquart, K.H., Luz, A., 1984. Oncogenic retrovirus from spontaneous murine osteomas. I. Isolation and biological characterization. *J. Gen. Virol.* 65 (Pt 12), 2237–2248.
- Sementchenko, V.I., Watson, D.K., 2000. Ets target genes: past, present and future. *Oncogene* 19 (55), 6533–6548.
- Speck, N.A., Renjifo, B., Golemis, E., Fredrickson, T.N., Hartley, J.W., Hopkins, N., 1990. Mutation of the core or adjacent LVB elements of the Moloney murine leukemia virus enhancer alters disease specificity. *Genes Dev.* 4 (2), 233–242.
- Steffen, B., Muller-Tidow, C., Schwable, J., Berdel, W.E., Serve, H., 2005. The molecular pathogenesis of acute myeloid leukemia. *Crit. Rev. Oncol. Hematol.* 56 (2), 195–221.
- Sørensen, K.D., Quintanilla-Martinez, L., Kunder, S., Schmidt, J., Pedersen, F.S., 2004. Mutation of all Runx (AML1/core) sites in the enhancer of T-lymphomagenic SL3-3 murine leukemia virus unmasks a significant potential for myeloid leukemia induction and favors enhancer evolution toward induction of other disease patterns. *J. Virol.* 78 (23), 13216–13231.
- Sørensen, K.D., Sørensen, A.B., Quintanilla-Martinez, L., Kunder, S., Schmidt, J., Pedersen, F.S., 2005. Distinct roles of enhancer nuclear factor 1 (NF1) sites in plasmacytoma and osteopetrosis induction by Akv1–99 murine leukemia virus. *Virology* 334 (2), 234–244.
- Thornell, A., Hallberg, B., Grundström, T., 1988. Differential protein binding in lymphocytes to a sequence in the enhancer of the mouse retrovirus SL3-3. *Mol. Cell. Biol.* 8 (4), 1625–1637.
- Thornell, A., Hallberg, B., Grundström, T., 1991. Binding of SL3-3 enhancer factor 1 transcriptional activators to viral and chromosomal enhancer sequences. *J. Virol.* 65 (1), 42–50.
- Wang, J.C., Dick, J.E., 2005. Cancer stem cells: lessons from leukemia. *Trends Cell Biol.* 15 (9), 494–501.
- Zaiman, A.L., Lenz, J., 1996. Transcriptional activation of a retrovirus enhancer by CBF (AML1) requires a second factor: evidence for cooperativity with c-Myb. *J. Virol.* 70 (8), 5618–5629.
- Zaiman, A.L., Nieves, A., Lenz, J., 1998. CBF, Myb, and Ets binding sites are important for activity of the core 1 element of the murine retrovirus SL3-3 in T lymphocytes. *J. Virol.* 72 (4), 3129–3137.